Res Chem Intermed (2016) 42:4055–4076
DOI 10.1007/s11164-015-2258-0

Removal of Th(IV), Ni(II)and Fe(II) from aqueous solutions by a novel PAN–TiO_2 nanofiber adsorbent modified with aminopropyltriethoxysilane

Mehdi Mokhtari[1] · **Ali Reza Keshtkar**[2]

Received: 16 May 2015 / Accepted: 3 September 2015 / Published online: 22 March 2016

Abstract A novel polyacrylonitrile (PAN)–titanium oxide (TiO_2) nanofiber adsorbent functionalized with aminopropyltriethoxysilane (APTES) was fabricated by electrospinning. The adsorbent was characterized by SEM, FTIR, TEG and BET analyses. The pore diameter and surface area of the adsorbent were 3.1 nm and 10.8 $m^2\ g^{-1}$, respectively. The effects of several variables, such as TiO_2 and amine contents, pH, interaction time, initial concentration of metal ions, ionic strength and temperature, were studied in batch experiments. The kinetic data were analyzed by pseudo-first-order, pseudo-second-order and double-exponential models. Two isotherm models, namely Freundlich and Langmuir, were used for analysis of equilibrium data. The maximum adsorption capacities of Th(IV), Ni(II) and Fe(II) by Langmuir isotherm were found to be 250, 147 and 80 mg g^{-1} at 45 °C with pH of 5, 6 and 5, respectively, and greater adsorption of Th(IV) could be justified with the concept of covalent index and free energy of hydration. Calculation of $\Delta G°$, $\Delta H°$ and $\Delta S°$ demonstrated that the nature of the Th(IV), Ni(II) and Fe(II) metal ions adsorption onto the PAN–TiO_2–APTES nanofiber was endothermic and favorable at a higher temperature. The negative values of $\Delta G°$ for Th(IV) showed that the adsorption process was spontaneous, but these values for Ni(II)and Fe(II) were positive and so the adsorption process was unspontaneous. Increasing of ionic strength improved the adsorption of Ni(II) and Fe(II) on nanofiber adsorbent but decreased the adsorption capacity of Th(IV). The adsorption capacity was reduced slightly after six cycles of adsorption–desorption, so the nanofiber adsorbent could be used on an industrial scale. The inhibitory effect of Ni(II) and Fe(II) on the

✉ Ali Reza Keshtkar
akeshtkar@aeoi.org.ir

[1] Department of Chemical Engineering, University of Tehran, Tehran, Iran

[2] Nuclear Fuel Cycle Research School, Nuclear Science and Technology Research Institute, Tehran, Iran

adsorption of Th(IV) was increased with an increase in the concentration of inhibitor metal ions.

Keywords Adsorption · Nanofiber · Electrospinning · PAN · TiO_2 · Heavy metals

Introduction

The heavy metals have very diverse applications and are commonly found in wastewater from the mining, metallurgical alloying, nuclear laboratories and nuclear fuel industry. Wastewater from these industries normally contains Th(IV), Fe(II), Ni(II) and other metals, and the presence of these metals in wastewater is of great concern because some of these metals are extremely toxic to human health and the environment [1]. Among these metals, thorium has a substantial half-life and so can stay in the human body and the environment for a long time. In addition, thorium has been extensively used in a variety of applications, which have some unwanted side effects because they produce various liquid and solid waste that can pollute the ground surface and underground waters [2]. So environmental engineers and scientists have been trying to find easy, effective, economical, and eco-friendly techniques for the removal of thorium and other heavy metals from wastewater [3]. Some processes for heavy metal removal are precipitation, adsorption [4–6], membrane processes [7, 8], electro-deionization [9], ion exchange [10] and extraction [11]. Among these, adsorption has been widely used because it is economically feasible, effective, simple and environmentally appropriate in practice [12, 13]. In recent years, nano-scale adsorbents have been extensively used for heavy metal ions adsorption because of their large specific surface area, regular pore structure and surface physical and chemical modification properties [14]. There are some nanoadsorbents such as nanobeads [15], nanocomposites [16] and nanofibers [14, 17, 18] that can be used for heavy metal removal. Among them, the polymer-based nanofiber adsorbents possess some specific properties such as large pore volume and specific surface area and facile production [19]. One of these polymers is PAN (polyacrylonitrile), which is a synthetic, semi-crystalline organic polymer with the linear formula $(C_3H_3N)_n$ and thermoplastic properties including not melting under normal conditions and degrading before melting, and melting above 300 °C if the heating rates are 50 °C/min or above [20]. In this investigation, the TiO_2 nanoparticles modified with the $–NH_2$ functional group of aminopropyltriethoxysilane (APTES) were selected because of their good adsorption properties. Many researchers have reported applications of TiO_2-based adsorbents for actual wastewater treatment [21–24]. Also, PAN was chosen as a polymeric matrix because of its good film-forming properties. Thus, the novel PAN–TiO_2–APTES nanofiber adsorbent was fabricated via the electrospinning method. The effects of both TiO_2 and APTES contents, pH, contact time, temperature, initial concentration and ionic strength on the performance of the nanofiber absorbent were investigated. In addition, some analyses such as SEM, FTIR, TEG and BET were carried out on the absorbent to investigate its quality. Furthermore, the adsorbent was revived with HCl/HNO_3 solution to study its desorption properties.

Experimental

Materials

Th(IV), Ni(II) and Fe(II) nitrate salts and PAN (MW = 150,000), APTES (99 %), acetone, HNO_3, NaOH, dimethyl sulfoxide (DMSO), HCl and NaCl salts were purchased from Merk (Germany). TiO_2 nanoparticles (size $\leq$20 nm) were provided by Sigma-Aldrich. Double-distilled water was prepared in the laboratory and used as a solvent of the metal salts, Th(IV), Ni(II), and Fe(II).

Equipment

The electrospinning system was used to fabricate the nanofibers. The ultrasonic apparatus was used to homogenize the PAN–TiO_2 polymer solution. The morphological analysis of the fabricated nanofibers was carried out using scanning electron microscopy (SEM). The adsorbent nanofibers were characterized by Fourier transform infrared spectroscopy (FTIR) (Vector 22; Bruker, Germany) in the range of 400–4000 cm^{-1}. The total pore volume, pore size and surface area were measured and calculated by BET (Brunauer–Emmett–Teller) analysis on the basis of the BJH (Brrett–Joyner–Halenda) method. The concentration of the remaining cations of Th(IV), Ni(II), and Fe(II) in the solution was measured by an ICP-AES (inductive coupled plasma atomic emission spectrometer). For determining the thermal behavior of the nanofibers, the TEG (thermal elastography) test was used.

Fabrication of the nanofibers

Fabrication of PAN nanofibers

For fabrication of PAN nanofiberthe , first 7 g of PAN was dissolved in 100 ml of DMSO at 25 °C and then the solution was stirred slowly for 24 h. After homogenizing the polymer solution with an ultrasonic device, the nanofibers were prepared using the electrospinning system under the following optimum conditions. The temperature, voltage, drum speed, distance between the drum and the needle and the polymer rate were: 25 °C, 21 kV, 500 rpm, 80 mm, and 2.5 mL h^{-1}, respectively.

Fabrication of PAN–TiO_2 nanofibers

The PAN–TiO_2 nanofibers were prepared by very slowly adding the TiO_2 nanoparticles to the PAN solution. The prepared solution was stirred for 2 h. For a comparative study of TiO_2 content, an adsorbent with different weight percentages (wt%) of nanoparticles (5, 10, 15, 20, 25) based on PAN content was prepared. For homogenous dispersion of the nanoparticles in the PAN solutions, the solutions

were separately sonicated for 45 min. Finally, the solutions were converted to composite nanofibers by electrospinning.

Fabrication of PAN–TiO_2–APTES nanofibers

PAN–TiO_2 nanofibers were modified by the amine functional groups to improve the adsorption capacity and to increase the active sites of the adsorbent. All steps were similar to the PAN–TiO_2 fabrication procedure, except for dissolving different weight percentages (10, 20, 30, 40, 50, 60) of APTES (based on PAN) and 20 % of TiO_2 (based on PAN) in 20 ml of DMSO and homogenizing the mixture with an ultrasonic device for 1 h. Finally, the solution was added to 7 wt% of PAN solution (based on DMSO) and mixed for 1 h. Then, the PAN–TiO_2–APTES nanofibers were fabricated by electrospinning.

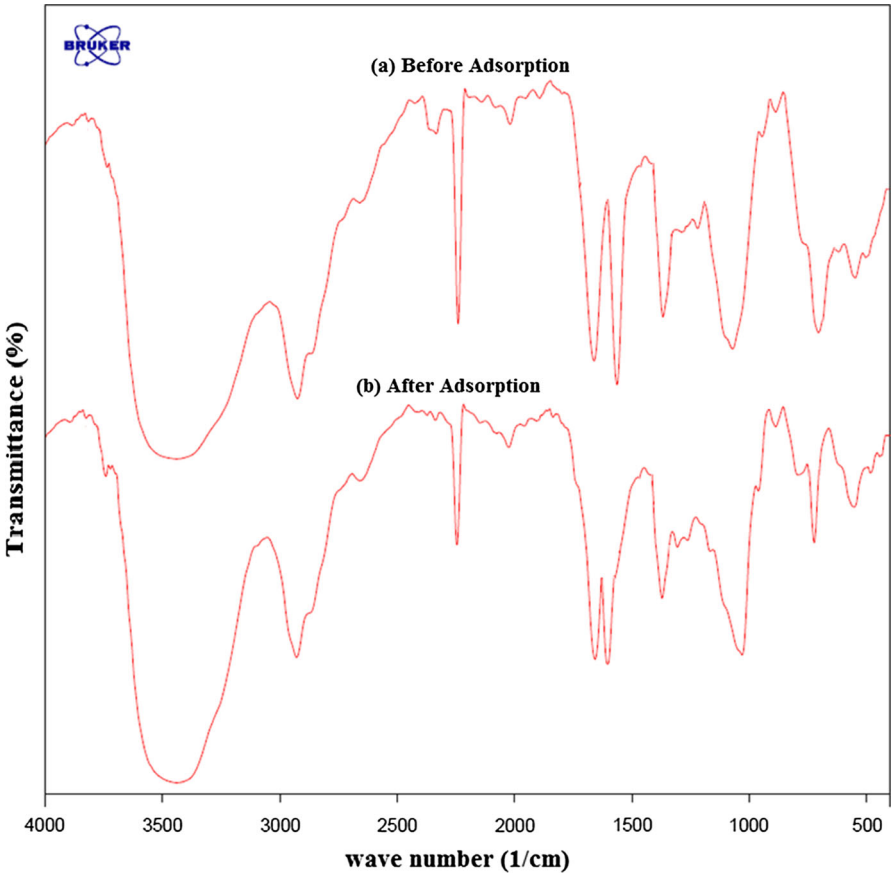

Fig. 1 FTIR spectra of PAN–TiO_2–APTES nanofiber (*a*) before heavy metal ion adsorption (*b*) after heavy metal ion adsorption

Adsorption experiments

All experiments were conducted in batch mode and in a 100-ml polyethylene flask, containing 0.05 g of adsorbent in 50 ml of metal solutions. The tests were done at 25 °C and at an optimum pH for each metal and initial metal concentration of 100 mg L^{-1}. This optimum pH for Th(IV), Ni(II), and Fe(II) was determined froman adsorption test which was performed at a fixed temperature (25 °C) and different pH ranging from 2 to 7. Adsorption kinetics was studied with an initial concentration of 100 mg L^{-1} of each metal ion, and at time intervals of 0–300 min at a temperature of 25 °C and optimum pH. To investigate the effect of the initial concentration of the metal ions, the adsorbent was rinsed in different metal ion solutions with concentrations in the range of 50–500 mg L^{-1} at three different temperatures (25, 35 and 45 °C). The amount of metal adsorbed was calculated as follows:

$$q_e = \frac{(C_i - C_e)V}{M} \quad (1)$$

where q_e is the equilibrium adsorption capacity (mg/g), C_i and C_e are initial and equilibrium concentrations (mg/l), respectively, V is the solution volume (l), and M is the adsorbent weight in the solution (g).

Results and discussion

Nanofiber characterization

The main functional groups of PAN–TiO_2–APTES nanofibers for adsorption of Th(IV), Ni(II) and Fe(II) were determined by the FTIR test. The FTIR spectra of

Table 1 The FTIR spectra characteristic of PAN–TiO_2–APTES before and after adsorption of heavy metals

Wave number (cm^{-1})				Assignment
Before adsorption	After adsorption	Displacement	Intensity change	
617–729	669–702	Positive	Weaken	Ti–O–Ti
943	977	Positive	Intensified	Si–OH (asymmetric)
889	871	Negative	No change	Si–OH (stretching)
2850–3049	2850–3049	Zero	Weaken	C–H
3510	3459	Negative	No change	–OH
2248	2248	Zero	Weaken	C ≡ N(nitrile)
1645	1645	Zero	Weaken	Amide
1548	1627	Positive	Weaken	Amine
1232	1245	Positive	Weaken	Methyl

PAN–TiO_2–APTES nanofibers before and after heavy metal adsorption are shown in Fig. 1. Also, the changes in band intensity and frequency after and before adsorption are given in Table 1, which can be used to identify the functional groups involved in the adsorption of heavy metals. The broad band in the range of 617–729 cm^{-1} corresponds to Ti–O–Ti stretching peaks which weaken and shift after the adsorption process which shows that these nanoparticles are effective in the adsorption process. The peaks at 943 and 889 cm^{-1} are because of the asymmetric bending and stretching vibration of Si–OH, respectively. These peaks shift after adsorption confirming the involvement of these groups in the adsorption process [14]. The bands in the region of 2850–3049 cm^{-1} are ascribed to the symmetric vibration of the C–H groups, and these peaks weaken after adsorption [25]. The vibration of –OH was observed around 3400–3500 cm^{-1}. The characteristic vibration band of the unconjugated nitrile group appeared at 2248 cm^{-1} and this peak weakened after adsorption, being evidence of the involvement of the nitrile group in the adsorption process [26]. The band around 1232 cm^{-1} can be assigned to the methyl groups, and after adsorption this band shifts and weakens. The peak at 1645 cm^{-1} can be assigned to the amide groups [26]. The banding vibration around 1548 cm^{-1} proves that secondary amine groups (N–H) have been successfully added to the PAN–TiO_2–APTES nanofiber adsorbent, and this peak weakens after the adsorption process and is displaced by 1627 cm^{-1} confirming that the (N–H) functional group participates in the adsorption process [27]. The results indicate that

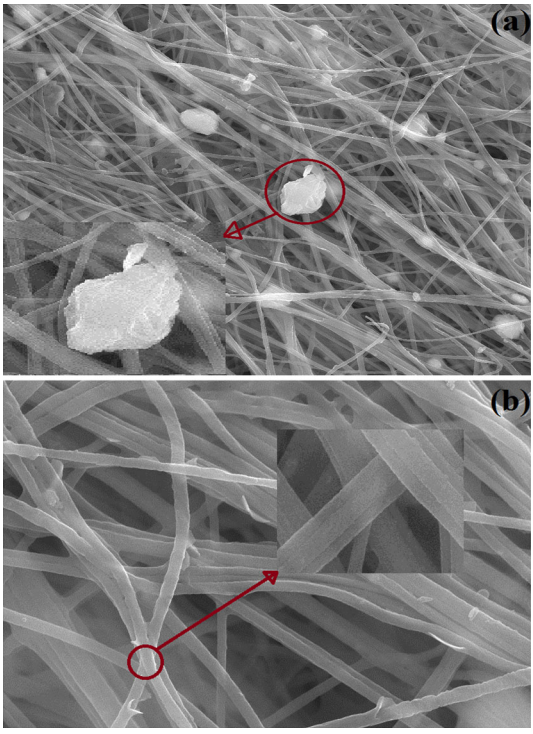

Fig. 2 SEM images of the fabricated nanofibers PAN–TiO_2 (25 wt%) (**a**) and PAN–TiO_2 20 wt%–APTES 50 wt% (**b**)

the chemical interactions between the hydroxyl, nitrile and amine groups of nanofiber adsorbent and the metal ions are mainly involved in the adsorption process. These observations confirm that the chemical interaction is one of the main mechanisms of adsorption.

The effects of TiO_2 nanoparticles on the morphology of composite nanofibers were studied by SEM images. Typical surface SEM photographs of PAN–TiO_2 25 wt% and PAN–TiO_2 20 wt%–APTES 50 wt% nanofiber adsorbents are illustrated in Fig. 2. Figure 2a shows that PAN–TiO_2 25 wt% nanofiber adsorbent is aggregated with the nanoparticles, and hence beads are observable. In contrast, as can be seen in Fig. 2b, there are no beads of the TiO_2 nanoparticles in the PAN–TiO_2 20 wt%–APTES 50 wt% nanofiber adsorbents. This image also shows that the modified TiO_2 with the amine groups has excellent adhesion and strong interfacial bonding to the PAN polymer [28].

Based on the BJH method, a narrow pore-size distribution is observed for the PAN–TiO_2–APTES nanofiber adsorbent with an average pore size of 3.1 nm and total pore volume of 0.038 $cm^3\ g^{-1}$; the pore diameter distribution plot for PAN–TiO_2–APTES nanofiber adsorbent is shown in Fig. 3. BET analysis showed that the surface area of the PAN–TiO_2–APTES nanofibers was 10.8 $m^2\ g^{-1}$. Based on the BJH theory, the pore diameters of the fibers were found to be 3.1 nm. Hence, the surface of the PAN–TiO_2–APTES nanofiber adsorbents was mesoporous. For the specification of adsorbent thermal characteristics, the TEG test was carried out from ambient temperature to 500 °C, using an ascending temperature rate of 10 °C/min. Figure 4 shows the thermal strength of the adsorbent against sublimation and

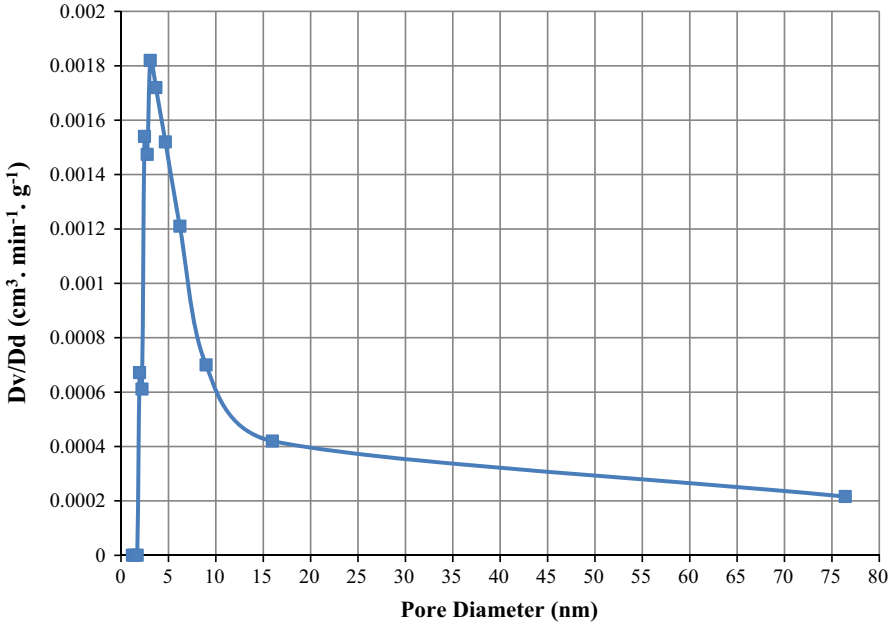

Fig. 3 Pore diameter distribution plot for the PAN–TiO_2–APTES nanofiber adsorbent

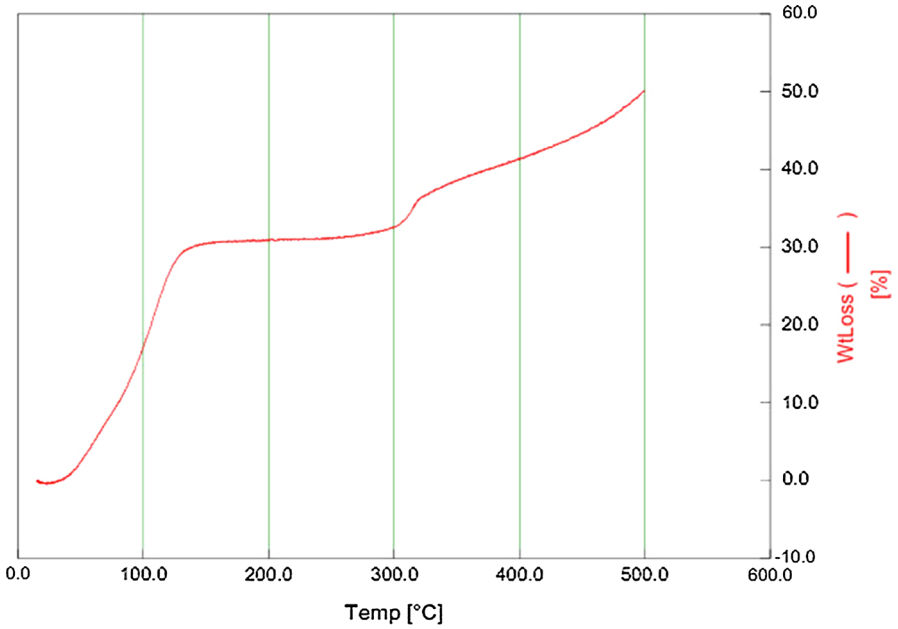

Fig. 4 TEG analysis of the PAN–TiO2–APTES nanofibers from ambient temperature to 500 °C

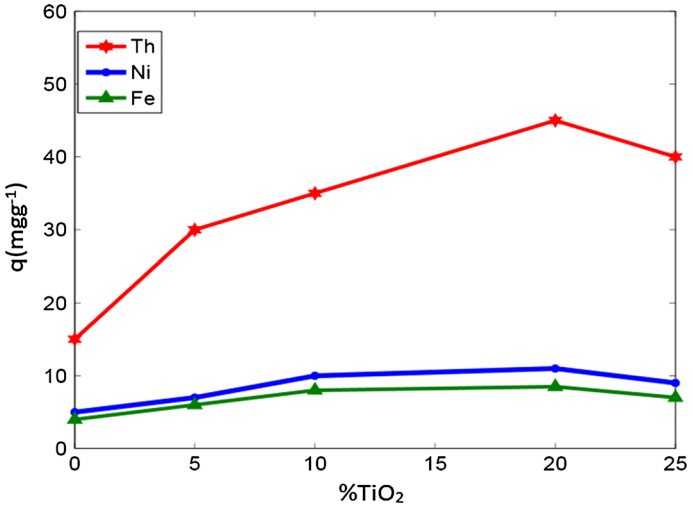

Fig. 5 Effect of the TiO_2 weight percentage in the PAN–TiO_2 nanofiber adsorbent on athe dsorption of Th(IV), Ni(II) and Fe(II) ions

vaporization. As shown in Fig. 4, the initial rate of weight loss of the nanofibers is rapid because of the remaining DMSO, but after vaporization of the DMSO by increasing the temperature to 500 °C, only 50 % of the nanofiber was vaporized;

this is because the base of the PAN–TiO_2–APTES nanofibers is PAN. These nanofibers have a great thermal strength.

Effect of TiO_2 on the adsorption

The effect of the TiO_2 weight percent on the adsorption capacity of Th(IV), Ni(II) and Fe(II) ions onto the PAN–TiO_2 nanofibers was investigated with a pH of 5, initial concentration 100 mg L^{-1}, adsorbent dosage 1 g L^{-1}, temperature of 25 °C, and in different amounts of TiO_2 (0, 5, 10, 15, 20, 25 wt%, based on the PAN weight). The capacity of adsorption of Th(IV), Ni(II) and Fe(II) ions onto PAN–TiO_2 nanofibers is shown in Fig. 5. As can be seen in Fig. 5, the adsorption capacity of Th(IV), Ni(II) and Fe(II) ions increases with an increase in TiO_2 amounts up to 20 wt%, and this increase is considerably greater for Th(IV) than for Ni(II) and Fe(II). This growth, which is about 200, 100 and 90 % for Th(IV), Ni(II) and Fe(II), respectively, is due to a large number of active sites on the adsorbent. These results show that the TiO_2 nanoparticles synergistically improve the adsorption capacity of metal ions onto the PAN nanofiber adsorbent. Similar trends were reported by other researchers [14, 18]. Further increases in TiO_2 amounts causes a decrease in the adsorption capacity of the nanofiber adsorbent for the three metal ions. This decrease can be because of the agglomeration and coagulation of TiO_2 nanoparticles which decrease the available surface of the adsorbent. Furthermore, the aggregation of nanoparticles causes the Th(IV), Ni(II) and Fe(II) ions to barely diffuse in the pores on the internal surface of the nanofiber [29]. So, PAN–TiO_2 (20 wt%) nanofiber adsorbent was selected for the next stage of the adsorption studies.

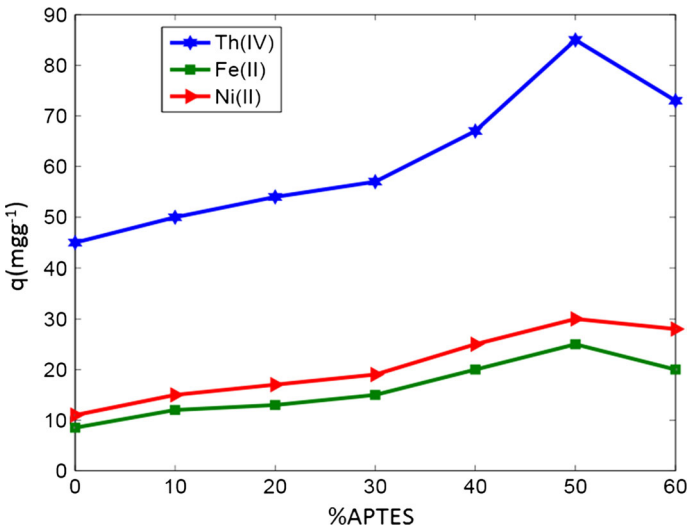

Fig. 6 Effect of APTES weight percentage in PAN–TiO_2–APTES nanofiber adsorbent on the adsorption of Th(IV), Ni(II) and Fe(II) ions

Effect of APTES on adsorption capacity

To study the effect of APTES content in nanofiber adsorbent on metal ions adsorption, PAN–TiO_2 20 wt% (based on PAN) nanofibers were functionalized with the amine groups ranging from 0 to 60 wt% of APTES with respect to the PAN weight. The adsorption capacity of Th(IV), Ni(II) and Fe(II) was studied at a pH of 5, initial concentration of 100 mg L^{-1}, adsorbent concentration of 1 g L^{-1} and temperature of 25 °C. Figure 6 shows that the adsorption capacity of T(IV), Ni(II)and Fe(II) ions increases with an increase in APTES amounts up to 50 wt%, and reaches 85, 30 and 25 mg g^{-1} for Th(IV), Ni(II) and Fe(II), respectively. This increase is because of the great affinity of the amine groups to interact with the metal ions, as well as the more uniform surface and more regular pore structure. Further increases in APTES amounts cause a decrease in the adsorption capacity of the Th(IV), Ni(II) and Fe(II) ions. This decrement can be due to a decrease in surface area and pore volume which reduces the active sites of PAN–TiO_2–APTES nanofibers for the adsorption process. So, PAN–TiO_2 20 %–APTES 50 % nanofibers were selected for further experiments.

Ascertaining of pH_{pzc}(point of zero charge)

The pH_{pzc} for the PAN–$TiO_2$20 %–APTES50 % nanofiber adsorbent was determined as follows: A series of 100-mL water flasks was prepared and their pH was adjusted in the range of 1–6 by adding 0.1 M HCl and/or 0.1 M NaOH solution. Then, 0.1 g of the adsorbent was added to each solution. These flasks were kept for 2 days. Finally, the pH of the solutions was measured. pH_{pzc} was reported as the pH at which the initial pH equaled the final pH; the obtained pH_{pzc} was equal to 3.1 for these nanofibers.

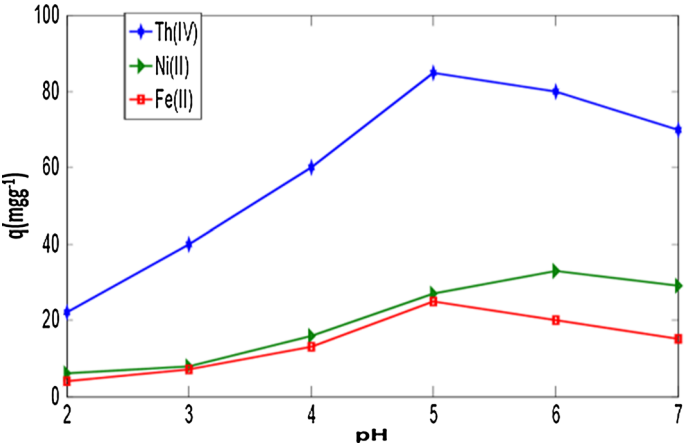

Fig. 7 Effect of pH on the Th(IV), Ni(II) and Fe(II) adsorption onto the PAN–TiO_2–APTES nanofiber adsorbent

Effect of pH

Solution pH is an important factor for the adsorption experiments. The values of the capacity of adsorption of Th(IV), Ni(II) and Fe(II) ions onto the PAN–TiO_2–APTES nanofiber adsorbent as a function of pH are shown in Fig. 7. As can be seen, the adsorption capacities are found to be low at low pH values and increase with an increase in pH, and then decrease as the pH continues ascending. The results show that the pH has a stronger effect on Th(IV) adsorption than on the Ni(II) and Fe(II) adsorption. At a low pH, because H_3O^+ is in competition with the Th(IV), Ni(II) and Fe(II) ions, the nanofiber surface takes up more H_3O^+, reducing the heavy metal ions bound to the adsorbent surface. H_3O^+ ions hinder the access of the metal ions from the surface functional groups such as amine (–NH). As can be seen from Fig. 7, the amount of Th(VI), Ni(II) and Fe(II) ions adsorption onto the PAN–TiO_2–APTES nanofiber adsorbent increases with the increasing pH up to an optimum pH because the competition between the H_3O^+ ions and heavy metal ions decreases. The optimum pH with which the adsorption capacity is at a maximum is 5, 6 and 5 for Th(IV), Ni(II) and Fe(II) ions, respectively. At pH greater than the optimum value, the formation of anionic hydroxide complexes reduces the concentration of the free heavy metal ions, so the adsorption capacity of the metal ions decreases [14, 30, 31]. The observed relationship can be explained by the effect of the surface charge of nanofiber adsorbent and pH_{pzc}. At $pH < pH_{pzc}$, the nanofiber surface is positive, and as a result, the electrostatic repulsion between the positive charge on the nanofibers and the metal ions reduces the adsorption capacity. When $pH > pH_{pzc}$, the nanofiber surface has a negative charge, which increases the attractive force between the metal ions and the nanofibers, and increases the power of complex formation of the functional group with the metal ions, so the adsorption capacity increases.

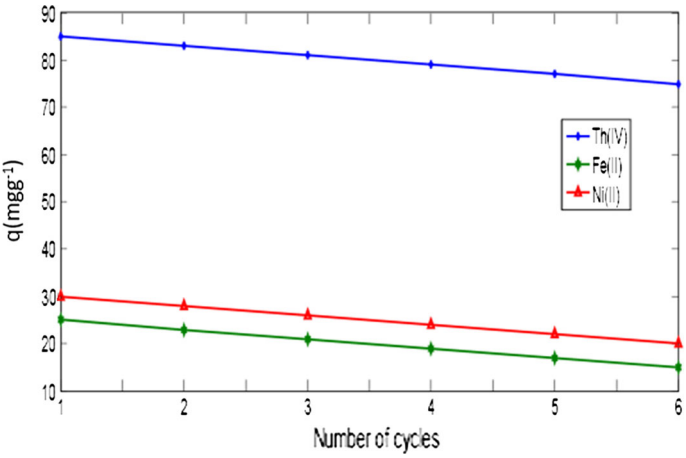

Fig. 8 Six cycles of Th(IV), Ni(II) and Fe(II) sorption–desorption with 0.5 M HNO3/0.1 M HCl in an equal ratio solution

Regeneration of PAN–TiO_2–APTES nanofiber adsorbent

Regeneration of the adsorbent for repeated uses and economic issues is an important factor in industrial practice for metal removal from wastewater. For desorption of Th(IV), Ni(II) and Fe(II) ions from the PAN–TiO_2–APTES nanofiber adsorbent, 0.5 M HNO_3/0.1 M HCl in an equal ratio solution at a temperature of 25 °C and contact time of 4.5 h was used as a desorbing agent [14]. Also, the adsorption process of each metal ion was carried out at a pH of 5 and initial metal ion concentration of 100 mg L^{-1}. As observed in Fig. 8, the capacity of adsorption of Th(IV), Ni(II) and Fe(II) ions onto the adsorbent reduced from 85, 30 and 25 mg g^{-1} in the first step to 80, 25 and 19 mg g^{-1} in the sixth step, respectively. This shows that PAN–TiO_2–APTES nanofiber adsorbent can be used on an industrial scale without any significant loss in adsorption performance. The slight reduction of the adsorption capacity of the adsorbent is due to physical reduction of some –NH functional groups by the acid rupture [14].

Effect of interaction time and kinetics of adsorption

The profiles of adsorption of Th(IV), Ni(II) and Fe(II) ions onto PAN–TiO_2–APTES adsorbent as a function of time are presented in Fig. 9. The adsorption of metal ions rapidly increases in the first 120 min and then adsorption slowly approaches equilibrium, because in the first 120 min all active sites on the adsorbents surface are vacant and the solution concentration is high. After this time, few active sites on the adsorbent are available, so the adsorption rate of the metal ions decreases.

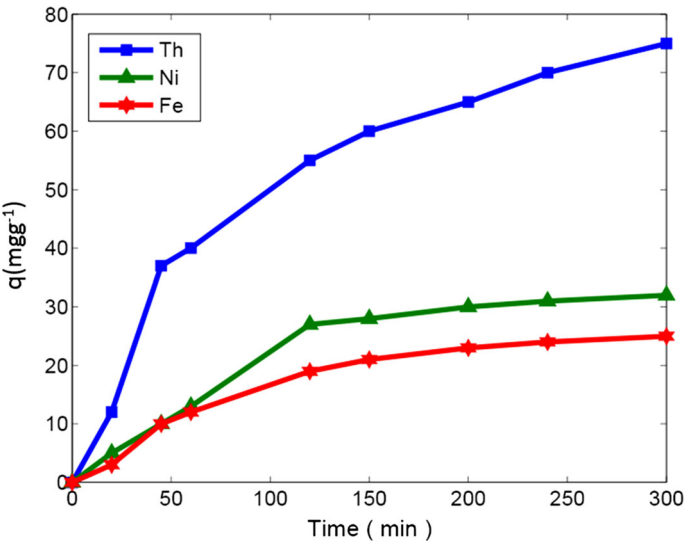

Fig. 9 Effect of interaction time on Th(IV), Ni(II) and Fe(II) adsorption onto the PAN–TiO_2–APTES nanofiber adsorbent

Table 2 Kinetic parameters for Th(IV), Ni(II) and Fe(II) adsorption onto the PAN–TiO_2–APTES nanofiber adsorbent

Metal	q_{exp} (mg g^{-1})	K_1 (min^{-1})	q (mg g^{-1})	R^2
Pseudo-first-order				
Th(IV)	85	0.013321	84.3	0.9910
Ni(II)	32	0.012013	31.5	0.9879
Fe(II)	25	0.012431	23.7	0.9899
Metal	q_{exp} (mg g^{-1})	K_2 (gm g^{-1} min^{-1})	q (mg g^{-1})	R^2
Pseudo-second–order				
Th(IV)	*85*	0.000131	88.3	0.9023
Ni(II)	32	0.001623	32.0	0.9147
Fe(II)	25	0.001783	26.7	0.9972

Metal	q_{exp} (mg g^{-1})	D_1 (g L^{-1})	K_{D1} (min^{-1})	D_2 (g L^{-1})	K_{D2} (min^{-1})	q (mg g^{-1})	R^2
Double-exponential model							
Th(IV)	85	28.31	0.032	58.27	0.005	85.0	0.9912
Ni(II)	32	1.88	0.024	1.93	0.024	31.5	0.9935
Fe(II)	25	12.58	0.052	11.52	0.014	24.6	0.9968

Adsorption kinetics is one of the most important features of the adsorption process. Kinetic models describe the mechanism of the adsorption process. The experimental data were studied using three kinetic models including pseudo-first-order, pseudo-second-order and double-exponential [32, 33] by non-linear fitting using the MATLAB software.

$$\text{Pseudo-first-order}: \quad q_t = q_e(1 - exp(-kt)) \tag{2}$$

$$\text{Pseudo-second-order}: \quad q_t = \frac{K_2 q_e^2 t}{1 + K_2 q_e t} \tag{3}$$

$$\text{Double-exponential model}: \quad q_t = q_e - \frac{D_1}{m_{ads}}\exp(-k_{D1}t) - \frac{D_2}{m_{ads}}\exp(-k_{D2}t) \tag{4}$$

where q_t and q_e (mg g^{-1}) are the amounts of Th(IV), Ni(II) and Fe(II) adsorbed on PAN–TiO_2–APTES nanofiber adsorbent at time t and equilibrium, respectively; k_1 (min^{-1}) is the pseudo-first-order rate constant, k_2 (gm g^{-1} min^{-1}) is the pseudo-second-order rate constant, k_{D1} and k_{D2} (min^{-1}) are the double-exponential rate constants, m_{ads} (g L^{-1}) is the adsorbent concentration, and D_1 and D_2 (g L^{-1}) are the equation constants which correspond to the rapid phase and the slow phase, respectively [34]. For the pseudo-first-order and the pseudo-second-order kinetic models, physical and chemical surface adsorption, respectively, could be considered as the rate-controlling step. The double-exponential kinetic model forecasts the kinetic behavior of the adsorption by which the diffusion phenomenon has been a

rate-controlling step. The value of the constants can be obtained from the non-linear regression analysis as given in Table 2. The results show that the coefficient of correlation (R^2) for the double-exponential kinetic model is higher than 0.99 for all metal ions, and the calculated values of q_e for the double-exponential model is very close to the experimental values. So, it is obvious that the kinetic data were best fitted with the double-exponential kinetic model. This model shows that the adsorption process takes place in two steps: transport of the metal ions to the exterior surface of the nanofiber as a rapid phase, and adsorption of the metal ions on the internal surface of the adsorbent as a slow phase.

Effect of initial concentration and temperature

The change in adsorption behavior of the PAN–TiO_2–APTES nanofiber adsorbent with different metal ions concentrations from 50 to 500 mg L^{-1} is shown in Fig. 10, from which it can be seen that the adsorption capacity of the nanofiber adsorbent increases from 44, 10 and 7 to 230, 85 and 75 mg g^{-1}, respectively, at 25 °C with increasing initial concentrations of the Th(IV), Ni(II) and Fe(II) ions. This uptrend may be because of an increase in the initial ion concentration creating a greater driving force to overcome the whole mass transfer resistance between the solid and liquid phases, so this leads to an increase in adsorption of heavy metals. In order to study the effects of temperature on the capacity of adsorption of Th(IV), Ni(II) and Fe(II) ions onto the PAN–TiO_2–APTES nanofiber adsorbent, the experiments were carried out at different temperatures (25–45 °C), the results of which are shown in Fig. 10. As can be seen, the adsorption capacity ascends with increasing temperature for all three metal ions. This may be because of the mounted mobility of the heavy metal ions and their tendency to be adsorbed from the aqueous solution onto the surface of the nanofiber adsorbent as well as a powerful activity of binding sites because of the increasing temperature [18]. The result may lead to more interactions between the Th(IV), Ni(II) and Fe(II) ions and active sites on the PAN–TiO_2–APTES nanofiber adsorbent [33]. As shown in Fig. 10, there is a significant difference between Th(IV) adsorption and Ni(II) and Fe(II) adsorption capacity at all initial concentrations and temperatures. This phenomenon can be justified by the concept of free energy of hydration and covalent index. The free energy of hydration and covalent index amounts can be calculated from Eqs. 5 and 6 [34, 35]

$$\text{Free energy of hydration} = \frac{-69500Z_c^2}{r} \tag{5}$$

$$\text{Covalent index} = X_m r^2 \tag{6}$$

where Z_c, r and X_m are cation charge, atomic radius and electronegativity, respectively. These amounts and calculated free energy of the hydration and covalent index are given in Table 3. When the free energy of hydration for a metal is high, the tendency for that metal to remain in liquid phase is greater than moving towards the adsorbent structure. According to Table 3, the order of the free energy of hydration for metals is as follows: Fe(II) > Ni(II) > Th(IV), so the Fe(II) and Ni(II)

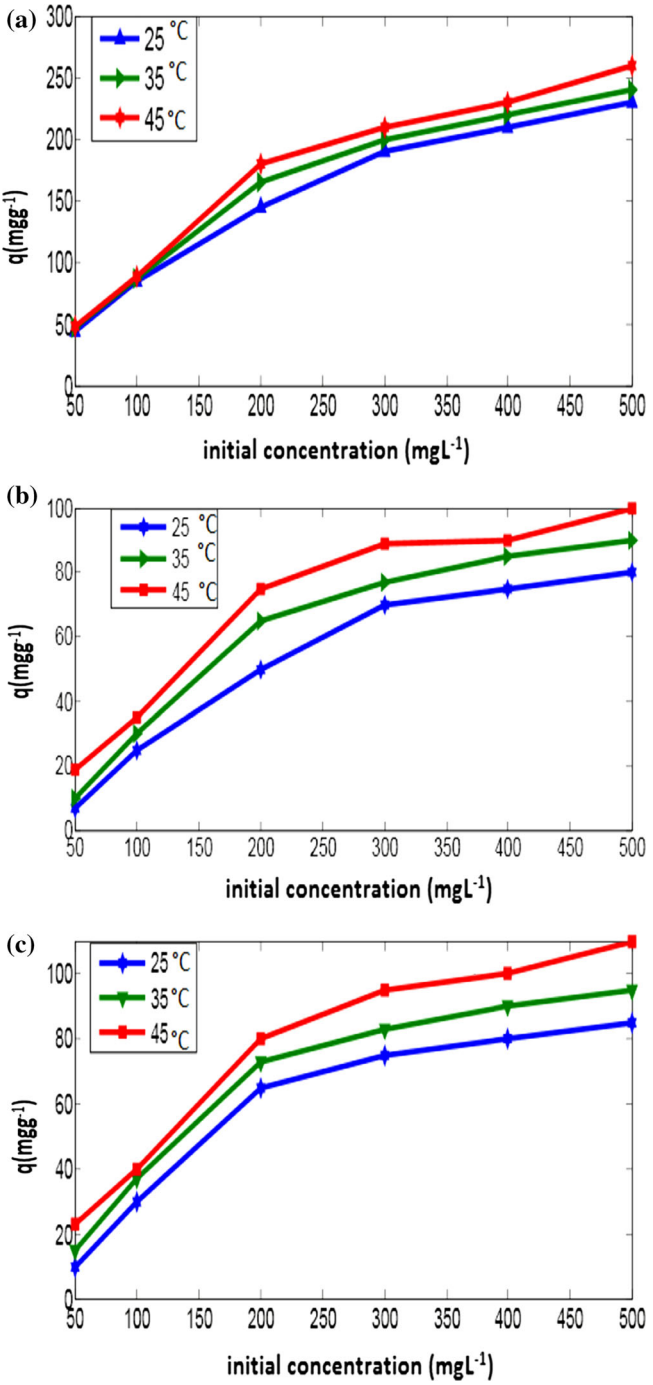

Fig. 10 Effect of initial concentration and temperature on Th(IV) (**a**), Ni(II) (**b**) and Fe(II) (**c**) adsorption onto the PAN–TiO_2–APTES nanofiber adsorbent

complexes tend to remain in liquid phase and Th(IV) complexes tend to enter the adsorbent and solid phase. Also, the metals with the higher covalent index adsorb more readily. Therefore, Th(IV) adsorption is more than Ni(II), and Ni(II) is more than Fe(II).

Adsorption isotherms

To explain the adsorption process as a function of the equilibrium concentration in an aqueous solution and to provide a better conception of the mechanism of adsorption, the Langmuir and Freundlich isotherm models were studied at three different temperatures (25, 35 and 45 °C). Parameters of these isotherm models at different temperatures were calculated and the results are given in Table 4. The Langmuir model approximates the maximum adsorption capacity corresponding to complete monolayer coverage on the adsorbent surface. This model presumes that the surface is homogeneous and that the energy of adsorption is constant. The linearized form of the Langmuir isotherm model is given in the following equation [36]:

$$\text{Langmuir}: \frac{C_e}{q_e} = \frac{1}{q_{\max} K_L} + \frac{C_e}{q_{\max}} \tag{7}$$

where C_e (mg L^{-1}) is the equilibrium concentration of the metal ions, q_e (mg g^{-1}) is the amount adsorbed in equilibrium in mg g^{-1} and q_m (mg g^{-1}) is the parameter related to maximum adsorption capacity. K_L (L mg^{-1}) is a constant related to the energy of adsorption. As can be seen in Table 4, the maximum adsorption capacities based on the Langmuir model at a temperature of 45 °C are 250, 147 and 80 mg g^{-1} for Th(IV), Ni(II) and Fe(II), respectively. The Freundlich isotherm is an equation which indicates heterogeneous surface adsorption with non-uniform energies of active sites. The linearized form of this model can be expressed as follows [37]:

$$\text{Freundlich}: Ln(q_e) = Ln(K_F) + \frac{1}{n} Ln(C_e) \tag{8}$$

where K_F (mg g^{-1}) and 1/n are Freundlich constants related to the adsorption capacity and adsorption intensity, respectively. As observed in Table 4, for all studied temperatures, the n values are more than the unit, showing a favorable adsorption of Th(IV), Ni(II) and Fe(II) on the surface of the adsorbent.

By comparison of the correlation coefficients (R^2 values), it was seen that the Langmuir model fitted the equilibrium data better than the Freundlich model due to the homogeneous distribution of active sites on the PAN–TiO_2–APTES nanofiber adsorbent. The maximum adsorption capacities of the Th(IV), Ni(II) and Fe(II) ions

Table 3 Free energy of hydration; covalent index for Th(IV), Ni(II) and Fe(II)

Metal	Z_C	Rpm	X_m Free energy of hydration (KJ mol^{-1})	Covalent index
Th(IV)	4	179	1.30–6212	41653
Ni(II)	2	124	1.91–2242	29,368
Fe(II)	2	126	1.83–2206	29,053

onto the PAN–TiO_2–APTES nanofiber adsorbent are compared with those of the other adsorbents reported in the literature in Table 5. As can be seen, the maximum adsorption capacities of the Th(IV), Ni(II) and Fe(II) ions onto the nanofiber are in the range of the maximum adsorption capacities of other adsorbents.

Thermodynamic analysis of process

Changing temperature has some effects on adsorption; if formulated, this change would be aligned with some important factors, such as enthalpy change (ΔH°), free energy of Gibbs change (ΔG°), entropy change (ΔS°) and equilibrium adsorption constant (K_c). K_c at three temperatures, 25, 35 and 45 °C, was obtained from the following equation by plotting C_{es}/C_{el} versus C_{el} [31].

$$K_c = \lim_{C_e \to 0} \frac{C_{es}}{C_{el}} \tag{9}$$

where C_{el} and C_{es} are metal equilibrium concentrations in liquid and solid phases, respectively. Standard free energy of Gibbs (ΔG°) could be calculated from the following equation:

Table 4 Langmuir and Freundlich constants for Th(IV), Ni(II) and Fe(II) adsorption onto the PAN–TiO_2–APTES nanofiber adsorbent

Metal	Temperature (°C)	q_m (mg g^{-1})	K_L (L mg^{-1})	R^2
Langmuir isotherm				
Th(IV)	25	220	0.052	0.998
	35	229	0.095	0.998
	45	250	0.123	0.998
Ni(II)	25	70	0.025	0.916
	35	134	0.027	0.949
	45	147	0.032	0.974
Fe(II)	25	70	0.021	0.970
	35	75	0.022	0.975
	45	80	0.025	0.990
Metal	Temperature (°C)	n	K_F (mg g^{-1})	R^2
Freundlich isotherm				
Th(IV)	25	2.42	24.42	0.965
	35	3.23	34.41	0.970
	45	3.54	45.15	0.971
Ni(II)	25	1.81	3.26	0.864
	35	1.98	5.34	0.884
	45	2.09	6.74	0.923
Fe(II)	25	1.53	1.58	0.914
	35	1.61	2.84	0.890
	45	2.14	4.84	0.915

Table 5 Comparison of adsorption capacity (mg g^{-1}) of the PAN–TiO_2–APTES nanofiber adsorbent for Th(IV), Ni(II) and Fe(II) adsorption with other adsorbents

Adsorbent	q_{Th} (mg g^{-1})	q_{Ni} (mg g^{-1})	q_{Fe} (mg g^{-1})	References
PVA–TiO_2–TMPTMS	238.1	–	–	[18]
Unmodified Nigerian kaolinite clay	–	166.67	–	[38]
Bacterially produced metal sulfides(BPMS)	–	15	17	[39]
PVA–TiO_2–APTES	–	13.01	–	[40]
Coconut dregs residue	–	64	–	[41]
Polyacrylamide-expanded perlite	171.68	–	–	[42]
Aminated PAN–SiO_2 nanofiber	249.4	69.5	–	[14]
PAN–TiO_2–APTES	250	147	80	This research

Table 6 Thermodynamic parameters for Th(IV), Ni(II) and Fe(II) adsorption onto the PAN–TiO_2–APTES nanofiber adsorbent

Metal	K_c			ΔH° (KJ mol^{-1})	ΔS° (KJ mol^{-1} K^{-1})	ΔG° (KJ mol^{-1})		
	25 °C	35 °C	45 °C			25 °C	35 °C	45 °C
Th(IV)	23.32	30.31	49.23	37.17	0.145	−7.802	−8.734	−10.301
Ni(II)	0.46	0.53	0.64	25.44	0.094	1.923	1.625	1.179
Fe(II)	0.41	0.49	0.57	16.73	0.073	2.208	1.826	1.486

$$\Delta G^{\circ} = -RTln(K_C) \tag{10}$$

where R is the universal gas constant (8.314 J mol^{-1} K^{-1}). Entropy changes and enthalpy changes of adsorption process were calculated from the following equation by plotting $\ln(K_C)$ versus 1/T and from the slope and intercept of the plot.

$$\ln(K_C) = \frac{\Delta S^{\circ}}{R} - \frac{\Delta H^{\circ}}{R} \cdot \frac{1}{T} \tag{11}$$

These thermodynamic parameters are calculated and given in Table 6.

The negative values of $\Delta G°$ for Th(IV) show that the adsorption process for Th(IV) is spontaneous while it is not a spontaneous process for Fe(II) and Ni(II) due to the positive values of $\Delta G°$. The descending values of $\Delta G°$ with temperature confirm that the adsorption process for all three metals is more possible at higher temperatures. The positive values of enthalpy changes confirm that adsorption is an endothermic process for all three metals. Furthermore, the positive values of entropy for Th(IV), Ni(II) and Fe(II) show that disorder and randomness increase at the interface of the liquid and solid phases during the adsorption process.

Effect of ionic strength

The effect of ionic strength on the adsorption of Th(IV), Ni(II) and Fe(II) was investigated by adding the solution of NaCl and changing its concentration from 0 to 1 M at the initial metal concentration of 100 mg L^{-1} and a temperature of 25 °C and pH of 5. Figure 11 shows that adsorption of Ni(II) and Fe(II) are increased significantly because, by increasing the ionic strength, many complexes that have much potential for adsorption are created. Also, this increase could be referred to the increase of the thermodynamic activity of the metal ions and the decrease of the activity of water [43]. With an increase in the ionic strength, the adsorption capacity of Th(IV) is decreased, because some complexes that have a better potential for adsorption are apt to disappear.

Inhibitory effect of Ni(II) and Fe(II) on Th(IV) adsorption

Effect of intruder ions such as Ni(II) and Fe(II) on Th(IV) adsorption were studied by preparing binary mixture of Th(IV)- Ni (II) and Th(IV)- Fe(II) at a temperature of 25 °C and pH of 5. In these mixtures. Th(IV) concentration is fixed at 100 mg L^{-1}, whereas other heavy metal ions' concentrations change from 0 to 200 mg L^{-1}. As shown in Fig. 12, the presence of Ni(II) and Fe(II) ions retard the equilibrium adsorption of Th(IV) ion onto the PAN–TiO_2–APTES nanofiber adsorbent and reduce the adsorption capacity of Th(IV) from 85 to 65 and 60 mg g^{-1} in the presence of Fe(II) and Ni(II), respectively. As can be seen from Fig. 12, the inhibitory effect of Ni(II) ions is greater than that of Fe(II) ions on the Th(IV) adsorption.

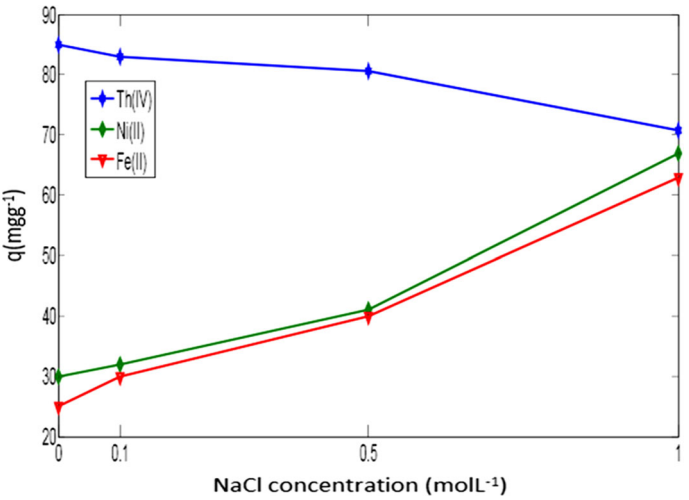

Fig. 11 Effect of ionic strength on Th(IV), Ni(II) and Fe(II) adsorption onto the PAN–TiO_2–APTES nanofiber absorbent

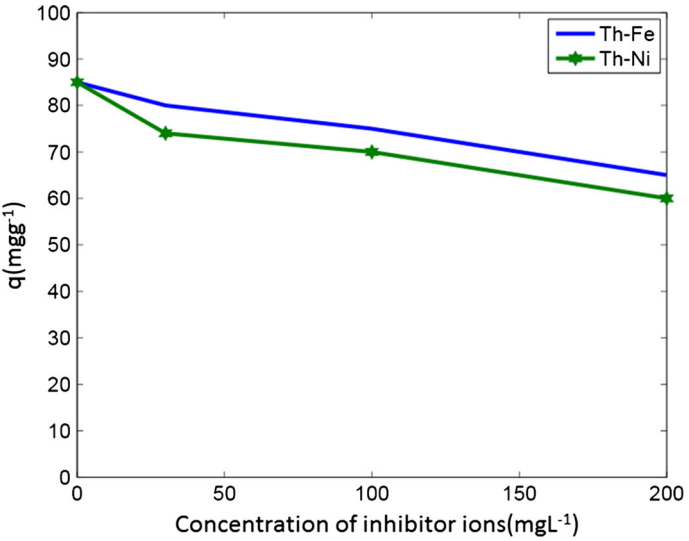

Fig. 12 Effect of concentration of inhibitor ions on the adsorption of Th(IV) onto the PAN–TiO_2–APTES nanofiber absorbent

Conclusion

The present study shows that the PAN–TiO_2–APTES nanofiber adsorbent is effective for the removal of Th(IV), Ni(II) and Fe(II) ions from aqueous solutions under optimized conditions of TiO_2 content (20 wt%), APTES content (50 wt%), pH (5, 6 and 5 for Th(IV), Ni(II) and Fe(II), respectively) and temperature (45 °C). FTIR spectra demonstrated that the PAN–TiO_2–APTES nanofiber adsorbent was functionalized successfully by amine groups. The BET analysis of the adsorbent base on the BJH method showed that the pore volume, pore diameter and surface area of the adsorbent were 0.038 $cm^3\ g^{-1}$, 3.1 nm and 10.8 $m^2\ g^{-1}$, respectively. The SEM images of the nanofiber adsorbents showed the effect of TiO_2 nanoparticles on the morphology of the PAN–$TiO_2$20 wt%–APTES50 wt% and PAN–TiO_2 25 wt% nanofibers, and some beads appeared in PAN–TiO_2 25 wt%. The adsorption kinetic studies indicated that the kinetic data were best fitted with the double-exponential kinetic model, with s regression coefficient of $R^2 > 0.99$. Among various isotherm models, the Langmuir isotherm model confirmed a better correlation with the experimental data which showed that the surface was homogeneous and the adsorption was monolayer. The maximum adsorption capacity from the Langmuir model for Th(IV), Ni(II) and Fe(II) were 250, 147 and 80 mg g^{-1} at 45 °C, respectively. The greater adsorption capacity for Th(IV) compared with Ni(II) and Fe(II) could be justified with the concept of the free energy of hydration and covalent index. The positive values of ΔH showed that for Th(IV), Ni(II) and Fe(II) the adsorption process was endothermic. Descending values of ΔG with the increase of adsorption temperature for Th(IV), Ni(II) and Fe(II) confirmed the better adsorption at a higher temperature. The positive values

of ΔG for Ni(II) and Fe(II) showed that the adsorption process for these metal ions was unspontaneous, while this value for Th(IV) was negative and the adsorption process was spontaneous. Increasing the solution ionic strength increased the adsorption of Ni(II) and Fe(II) metal ions, but decreased the adsorption of Th(IV) metal ions. Repeated adsorption–desorption cycles after six cycles showed that the nanofiber adsorbent, PAN–TiO_2–APTES, had a high potential in the removal and resumption of Th(IV), Ni(II) and Fe(II) ions from the wastewater. In the binary metal mixtures, the Th(IV) adsorption capacity reduced with increasing the concentration of the Ni(II) and Fe(II) inhibitor ions.

References

1. M.A. Barakat, New trends in removing heavy metals from industrial wastewater. Arab. J. Chem. **4**, 361–377 (2011)
2. M. Metaxas, Thorium removal by different adsorbents. J. Hazard. Mater. **97**, 71–82 (2003)
3. Y.C. Sharma, Economic treatment of cadmium (II)-rich hazardous waste by indigenous material. J. Colloid Interface Sci. **173**, 66–70 (1995)
4. M. Kilic, C. Kirbiyik, Ö. Cepeliogullar, A.E. Pütün, Adsorption of heavy metal ions from aqueous solutions by bio-char, a by-product of pyrolysis. Appl. Surf. Sci. **283**, 856–862 (2013)
5. S. Yari, S. Abbasizadeh, S.E. Mousavi, M.S. Moghaddam, A.Z. Moghaddam, Adsorption of Pb(II) and Cu(II) ions from aqueous solution by an electrospun CeO_2 nanofiber adsorbent functionalized with mercapto groups. Process Saf. Environ. Prot. **94**, 159–171 (2015)
6. M.R. Moghaddam, S. Fatemi, A. Keshtkar, Adsorption of lead (Pb^{2+}) and uranium cations by brown algae; experimental and thermodynamic modeling. Chem. Eng. J. **231**, 294–303 (2013)
7. R. Kumar, A.M. Isloor, Preparation and evaluation of heavy metal rejection properties of polysulfone/chitosan, polysulfone/N-succinyl chitosan and polysulfone/N-propylphosphonyl chitosan blend ultrafiltration membranes. Desalination **350**, 102–108 (2014)
8. W.P. Zhu, S.P. Sun, Dual-layer polybenzimidazole/polyethersulfone (PBI/PES) nanofiltration (NF) hollow fiber membranes for heavy metals removal from wastewater. J. Membr. Sci. **456**, 117–127 (2014)
9. S.Y. Huang, C.S. Fan, C. Hou, Electro-enhanced removal of copper ions from aqueous solutions by capacitive deionization. J. Hazard. Mater. **278**, 8–15 (2014)
10. A.M. Shoushtari, M. Zargaran, M. Abdouss, Preparation and characterization of high efficiency ion-exchange cross linked acrylic fibers. J. Appl. Polym. Sci. **101**, 2202–2209 (2006)
11. A.B. Resterna, R. Cierpiszewski, K. Prochaska, Kinetic and equilibrium studies of the removal of cadmium ions from acidic chloride solutions by hydrophobic pyridinecarboxamide extractants. J. Hazard. Mater. **179**, 828–833 (2010)
12. M. Visa, C. Bogatu, A. Duta, Simultaneous adsorption of dyes and heavy metals from multicomponent solutions using fly ash. Appl. Surf. Sci. **256**, 5486–5491 (2010)
13. D. Humelnicu, L. Bulgariu, M. Macoveanu, On the retention of uranyl and thorium ions from radioactive solution on peat moss. J. Hazard. Mater. **174**, 782–787 (2010)
14. A. Dastbaz, A. Keshtkar, Adsorption of Th^{4+}, U^{6+}, Cd^{2+} and Ni^{2+} from aqueous solution by a novel modified polyacrylonitrile composite nanofiber adsorbent prepared by electrospinning. Appl. Surf. Sci. **293**, 336–344 (2014)
15. D. Türkmen, E. Yılmaz, N. Ozturk, V. Akgol, A. Denizli, Poly(hydroxyethyl methacrylate) nanobeads containing imidazole groups for removal of Cu(II) ions. Mater. Sci. Eng. C **29**, 2072–2078 (2009)
16. X. Liu, Q. Hu, Z. Fang, X. Zhang, B. Zhang, Magnetic chitosan nanocomposites: a useful recyclable tool for heavy metal ion removal. Langmuir **25**, 3–8 (2009)
17. K. Saeed, S. Haidera, T.J. Oh, S.Y. Park, Preparation of amidoxime-modified polyacrylonitrile (PAN-oxime) nano-fibers and their applications to metal ions adsorption. J. Membr. Sci. **322**, 400–405 (2008)
18. S. Abbasizadeh, A.R. Keshtkar, M.A. Mousavian, Preparation of a novel electrospun polyvinyl alcohol/titanium oxide nanofiber adsorbent modified with mercapto groups for uranium(VI) and thorium(IV) removal from aqueous solution. Chem. Eng. J. **220**, 161–171 (2013)

19. H. Reneker, A.L. Yarin, Electrospinning jets and polymer nanofibers. Polymer **49**, 2387–2425 (2008)
20. A.K. Gupta, D.K. Paliwal, P. Bajaj, Polyacrilonitryle structure. J. Appl. Polym. Sci. **70**, 2703–2709 (1998)
21. M. Hua, S. Zhang, B. Pan, W. Zhang, L. Lv, Q. Zhang, Heavy metal removal from water/wastewater by nanosized metal oxides: a review. J. Hazard. Mater. **211–212**, 317–331 (2012)
22. X. Guan, J. Du, X. Meng, Y. Sun, B. Sun, Q. Hu, Application of titanium dioxide in arsenic removal from water: a review. J. Hazard. Mater. **215–216**, 1–16 (2012)
23. X. Qu, P.J.J. Alvarez, Q. Li, Applications of nanotechnology in water and wastewater treatment. Water Res. **47**, 3931–3946 (2013)
24. X. Zhao, L. Lv, B. Pan, W. Zhang, S. Zhang, Q. Zhang, Polymer-supported nanocomposites for environmental application: a review. Chem. Eng. J. **170**, 381–394 (2011)
25. A.R. Ladhea, P. Frailiea, D. Huab, M. Darsillob, D. Bhattacharyya, Thiol functionalized silica–mixed matrix membranes for silver capture from aqueous solutions: experimental results and modeling. J. Membr. Sci. **326**, 460–471 (2009)
26. G. Socrates, The theory of vibrational spectroscopy and its application to polymeric materials. Mater. Des. **3**, 646–647 (1982)
27. S. Deng, R. Bai, J.P. Chen, Aminated polyacrylonitrile fibers for lead and copper removal. Langmuir **19**, 5058–5064 (2003)
28. S. Mallakpour, A. Barat, Efficient preparation of hybrid nanocomposite coatings based on poly(vinyl alcohol) and silane coupling agent modified TiO_2 nanoparticles. Prog. Org. Coat. **71**, 391–398 (2011)
29. L. Ji, X. Zhang, Ultrafine polyacrylonitrile/silica composite fibers via electrospinning. J. Mater. Lett. **62**, 2161–2164 (2008)
30. C. Xiong, C. Yao, L. Wang, J. Ke, Adsorption behavior of Cd(II) from aqueous solutions onto geltype weak acid resin. Hydrometallurgy **98**, 318–324 (2009)
31. M. Irani, A. Keshtkar, M.A. Mousavian, Removal of cadmium from aqueous solution using mesoporous PVA/TEOS/APTES composite nanofiber prepared by sol–gel/electrospinning. Chem. Eng. J. **200–202**, 192–201 (2012)
32. F. Rashidi, R.S. Sarabi, Z. Ghasemi, A. Seif, Kinetic, equilibrium and thermodynamic studies for the removal of lead(II) and copper(II) ions from aqueous solutions by nanocrystalline TiO_2. Superlattices Microstruct. **48**, 577–591 (2010)
33. N. Chiron, R. Guilet, E. Deydier, Adsorption of Cu(II) and Pb(II) onto a grafted silica, isotherms and kinetic models. Water Res. **37**, 3079–3086 (2003)
34. K.T. Noa, Description of hydration free energy density as a function of molecular physical properties. Biophys. Chem. **78**, 127–145 (2005)
35. A. Zayed, M. Badruddozaa, Fe_3O_4/cyclodextrin polymer nanocomposites for selective heavy metals removal from industrial wastewater. Carbohydr. Polym. **91**, 322–332 (2013)
36. L.M. Zhou, Y.P. Wang, Z.R. Liu, Q.W. Huang, Characteristics of equilibrium, kinetics studies for adsorption of Hg(II), Cu(II), and Ni(II) ions by thiourea-modified magnetic chitosan microspheres. J. Hazard. Mater. **161**, 995–1002 (2009)
37. A. Taha, Y. Wu, H. Wang, F. Li, Preparation and application of functionalized cellulose acetate/silica composite nanofibrous membrane via electrospinning for Cr(VI) ion removal from aqueous solution. J. Environ. Manag. **112**, 10–16 (2012)
38. F.A. Dawodu, K.G. Akpomie, Simultaneous adsorption of Ni(II) and Mn(II) ions from aqueous solution onto a Nigerian kaolinite clay. J. Mater. Res. Technol. **3**, 129–141 (2014)
39. T. Jong, D.L. Parry, Adsorption of Pb(II), Cu(II), Cd(II), Zn(II), Ni(II), Fe(II), and As(V) on bacterially produced metal sulfides. J. Colloid Interface Sci. **275**, 61–71 (2004)
40. S. Abbasizadeh, A.R. Keshtkar, M.A. Mousavian, Sorption of heavy metal ions from aqueous solution by a novel cast PVA/TiO_2 nanohybrid adsorbent functionalized with amine groups. J. Ind. Eng. Chem. **20**, 1656–1664 (2014)
41. A. Kamari, S.N.M. Yusoff, F. Abdullah, W.P. Putra, Biosorptive removal of Cu(II), Ni(II) and Pb(II) ions from aqueous solutions using coconut dregs residue: adsorption and characterisation studies. J. Environ. Chem. Eng. **2**, 1912–1919 (2014)
42. R. Akkaya, Removal of radioactive elements from aqueous solutions by adsorption onto polyacrylamide–expanded perlite: equilibrium, kinetic, and thermodynamic study. Desalination **321**, 3–8 (2013)
43. M.K. Nazal, M.A. Albayyari, F.I. Khalili, Effect of high ionic strength on the extraction of uranium(VI) ions. J. Saudi Chem. Soc. **18**, 59–67 (2014)